Quantitative evaluation of lung injury caused by PM$_{2.5}$ using hyperpolarized gas magnetic resonance

Ming Zhang[1] | Haidong Li[1,2] | Hongchuang Li[1,2] | Xiuchao Zhao[1,2] | Qian Zhou[1,2] |
Qiuchen Rao[1] | Yeqing Han[1,2] | Yina Lan[3] | He Deng[1,2] | Xianping Sun[1,2] |
Xin Lou[3] | Chaohui Ye[1,2] | Xin Zhou[1,2] (iD)

[1]Key Laboratory of Magnetic Resonance in Biological Systems, State Key Laboratory of Magnetic Resonance and Atomic and Molecular Physics, National Center for Magnetic Resonance in Wuhan, Wuhan Institute of Physics and Mathematics, Innovative Academy of Precision Measurement Science and Technology, Chinese Academy of Sciences–Wuhan National Laboratory for Optoelectronics, Huazhong University of Science and Technology, Wuhan, People's Republic of China

[2]University of Chinese Academy of Sciences, Beijing, People's Republic of China

[3]Department of Radiology, Chinese PLA General Hospital, Beijing, People's Republic of China

Correspondence
Xin Zhou, Wuhan Institute of Physics and Mathematics, Innovative Academy of Precision Measurement Science and Technology, Chinese Academy of Sciences, 30 West Xiaohongshan, Wuhan, 430071, P. R. China.
Email: xinzhou@wipm.ac.cn

Purpose: To demonstrate the feasibility of ^{129}Xe MR in evaluating the pulmonary physiological changes caused by PM$_{2.5}$ in animal models.

Methods: Six rats were treated with PM$_{2.5}$ solution (16.2 mg/kg) by intratracheal instillation twice a week for 4 weeks, and another six rats treated with normal saline served as the control cohort. Pulmonary function tests, hyperpolarized ^{129}Xe multi-*b* diffusion-weighted imaging, and chemical shift saturation recovery MR spectroscopy were performed on all rats, and the pulmonary structure and functional parameters were obtained from hyperpolarized ^{129}Xe MR data. Additionally, histological analysis was performed on all rats to evaluate alveolar septal thickness. Statistical analysis of all the obtained parameters was performed using unpaired 2-tailed *t* tests.

Results: Compared with the control group, the measured exchange time constant increased from 11.74 ± 2.39 to 14.00 ± 2.84 ms ($P < .05$), and the septal wall thickness increased from 6.17 ± 0.48 to 6.74 ± 0.52 μm ($P < .05$) in the PM$_{2.5}$ cohort by ^{129}Xe MR spectroscopy, which correlated well with that obtained using quantitative histology (increased from 5.52 ± 0.32 to 6.20 ± 0.36 μm). Additionally, the mean TP/GAS ratio increased from 0.828 ± 0.115 to 1.019 ± 0.140 in the PM$_{2.5}$ cohort ($P = .021$).

Conclusions: Hyperpolarized ^{129}Xe MR could quantify the changes in gas exchange physiology caused by PM$_{2.5}$, indicating that the technique has the potential to be a useful tool for evaluation of pulmonary injury caused by air pollution in the future.

KEYWORDS
air pollution, gas exchange, hyperpolarized ^{129}Xe, lung injury, PM$_{2.5}$

1 | INTRODUCTION

Air pollution is a major environmental issue affecting respiratory health globally, especially in developing countries. Approximately 3.2 million people die from outdoor particulate matter (PM) pollution each year according to the global disease burden assessment in 2012.[1] Air pollution, characterized by a high level of PM, has become a major threat to public health in China.[2,3] Fine particulate matter ($PM_{2.5}$) is one of the most important air contaminants, with an aerodynamic diameter <2.5 μm, that could carry various toxic components and pathogens into the body attributable to its small diameter and large surface area.[4] Almost all $PM_{2.5}$ enters the body by the respiratory system, which is the site for gas exchange and is exposed directly to polluted air. Previous studies have found that $PM_{2.5}$ could increase the incidence of respiratory diseases, including pneumonia, asthma, chronic obstructive pulmonary disease (COPD), and lung cancers.[3,5-8]

Various methods have been previously reported to study pulmonary injury caused by $PM_{2.5}$. Lung physiological section analysis, bronchoalveolar lavage fluid (BALF) analysis, and enzyme-linked immunosorbent assay are the most widely used methods to analyze the physiological changes in the lung caused by $PM_{2.5}$. Thickening of alveolar wall and infiltration of neutrophils were observed in the lung injury model of $PM_{2.5}$ by hemotoxylin and eosin (H&E)-stained lung physiological sections.[9-12] Using the BALF method, total cell number, tumor necrosis factor alpha level, interleukin-6 level, lactate dehydrogenase level, and total protein level in BALF were also found to be higher in the model animals instilled with $PM_{2.5}$ solution than in control animals.[10-12] Additionally, synchrotron-based X-ray fluorescence has also been reported to study the mechanism of $PM_{2.5}$ toxicity to the lungs.[13] By using computed tomography (CT), a recent study found that $PM_{2.5}$ could increase the volume of peripheral, smaller blood vessels in the lungs, which may make people more prone to developing chronic lung disease.[14] These methods are effective to detect lung injury caused by $PM_{2.5}$, and the inflammatory response and oxidative stress damage of the lung can be quantified.[15] However, to the best of our knowledge, the effects of $PM_{2.5}$ on pulmonary perfusion have not been reported previously. Moreover, BALF, H&E-stained lung physiological sections, and other methods are invasive and cannot offer quantitative assessments of the pulmonary exchange function in vivo, greatly hindering their applications clinically, especially in diagnosing pulmonary diseases at the early stage.

Hyperpolarized ^{129}Xe MR has been proven to be a powerful tool to evaluate the pulmonary function and microstructure attributed to its extremely high MR sensitivity.[16-21] As a noninvasive, ionizing radiation-free technique, hyperpolarized ^{129}Xe MR enables quantifying the changes in pulmonary ventilation, microstructure, and gas exchange function, which have been widely used to study various lung diseases. Generally, hyperpolarized ^{129}Xe ventilation imaging could be utilized to quantify pulmonary ventilation defects in the lungs.[22,23] By applying models of diffusion, changes in the pulmonary microstructure caused by lung diseases, such as COPD, can be quantified by multi-b diffusion-weighted imaging (DWI)[24-27] and diffusion kurtosis imaging.[28] Additionally, hyperpolarized ^{129}Xe MR has unique advantages in exploring the gas exchange function of the lungs attributed to the increased chemical sensitivity to its surrounding environment and high solubility in tissue and blood. The chemical shifts of ^{129}Xe in the pulmonary tissue and plasma (TP) and red blood cells (RBCs) are 197 and 213 ppm, respectively, whereas that of the gas xenon in the alveoli is regarded as 0 ppm. Chemical shift saturation recovery (CSSR),[29-31] xenon polarization transfer,[32] and dissolved phase imaging[33,34] are the widely used techniques to evaluate the gas exchange function of the lung, obtained by measuring the exchange between dissolved and gaseous xenon in the lung. Hyperpolarized ^{129}Xe MR has been used to evaluate the microstructure and functional changes caused by pulmonary diseases, such as idiopathic pulmonary fibrosis, COPD, and radiation-induced lung injury.[35-39]

In this study, we aimed to demonstrate the feasibility of hyperpolarized ^{129}Xe MR to evaluate the physiological changes caused by $PM_{2.5}$ in animal models. Pulmonary function tests (PFTs) and quantitative histology analysis were used to compare the results of the hyperpolarized ^{129}Xe multiple b-value DWI and CSSR, which were used to obtain the microstructural and functional parameters of the lungs, respectively. All the experimental results were statistically analyzed between the experimental and control groups.

2 | METHODS

2.1 | ^{129}Xe polarization and delivery

Isotopically enriched xenon gas (86% ^{129}Xe) was polarized by spin-exchange optical pumping using a commercial polarizer system (verImagin Healthcare; Wuhan, China) and operated in continuous-flow mode. A total of 160 mL of hyperpolarized ^{129}Xe gas was cryogenically accumulated in 40 minutes and then was thawed into a Tedlar bag. The available spin polarization of the collected xenon gas was approximately 20%.

After polarization, xenon gas and oxygen were administered alternately to rat lung using a home-built MR-compatible hyperpolarized gas delivery system by the solenoid and pneumatic valves, which were controlled by a home-built LabVIEW program. Moreover, the pressure of the lung can be monitored in real time using an MR-compatible pressure sensor in the delivery system.

2.2 | PM₂.₅ sample preparation

The schematic of PM$_{2.5}$ sample collection and preparation is shown in Figure 1. First, the PM$_{2.5}$ sample was collected on the quartz fiber filter (WHA1851865; Whatman plc, Maidstone, UK) by a PM$_{2.5}$ cut point using a large-volume air particle sampler (TH-1000H; Wuhan Tianhong Instruments Co., Ltd., Wuhan, China) with a flow rate of 1.05 m^3/min. The PM$_{2.5}$ samples were collected in Wuhan, China from November 2017 to April 2018. After collection, the quartz fiber filters were cut into small pieces (5 × 5 mm^2), sonicated in ultrapure water for 180 minutes (30 min/time, 6 times), and then the solution was filtered using 8-layer sterile gauze. Thereafter, the PM$_{2.5}$ powder was extracted using a vacuum freeze dryer and then was suspended in normal saline (NS).[11,12,40-42] PM$_{2.5}$ size was measured using dynamic light scattering (ZEN3690; Malvern Instruments Ltd, Malvern, UK), and the average diameter was ~300 nm.

2.3 | Animal preparation

All the animal protocols were approved by the institutional animal care committee. Twelve male Sprague–Dawley rats (weight, 200 ± 20 g) were randomly divided into 2 groups (n = 6) after acclimatization. Six rats were treated with the PM$_{2.5}$ solution (16.2 mg/kg body weight, twice a week) for 4 weeks,[10,42] and the other rats treated with an equivalent

volume (0.6 mL) of NS served as the control group.[11] The PM$_{2.5}$ solution or NS was instilled into rat lungs by inserting a vein-detained needle (14 G) into the trachea carefully through its rima glottidis after anesthetization, as shown in Figure 1C.

In order to measure the actual effects of PM$_{2.5}$ on pulmonary physiology rather than the acute effects of instillation itself, MR experiments were performed on the seventh day after treatment.[13,41] Before the experiments, rats were anesthetized with 10% chloral hydrate and then were intubated with 14-G endotracheal tubes. Next, pulmonary function tests (PFTs) and hyperpolarized xenon MR experiments were performed in sequence on each rat. During the PFTs, rats breathed air spontaneously. In the MR experiments, rats were alternately ventilated with hyperpolarized xenon or oxygen using a home-built hyperpolarized xenon delivery system with a tidal volume of 2 or 1.6 mL, respectively.

2.4 | Pulmonary function tests

PFTs were performed on all the rats using a Forced Maneuvers system (CRFM 100; EMMS, Bordon, UK), and the parameters, including the forced vital capacity (FVC), forced expiratory volume (FEV), quasi-static compliance (Cchord), inspiratory capacity (IC), functional residual capacity (FRC), and total lung capacity (TLC), defined as FRC + IC, were obtained. All the PFTs were finished in 5 minutes after connection to the plethysmograph.
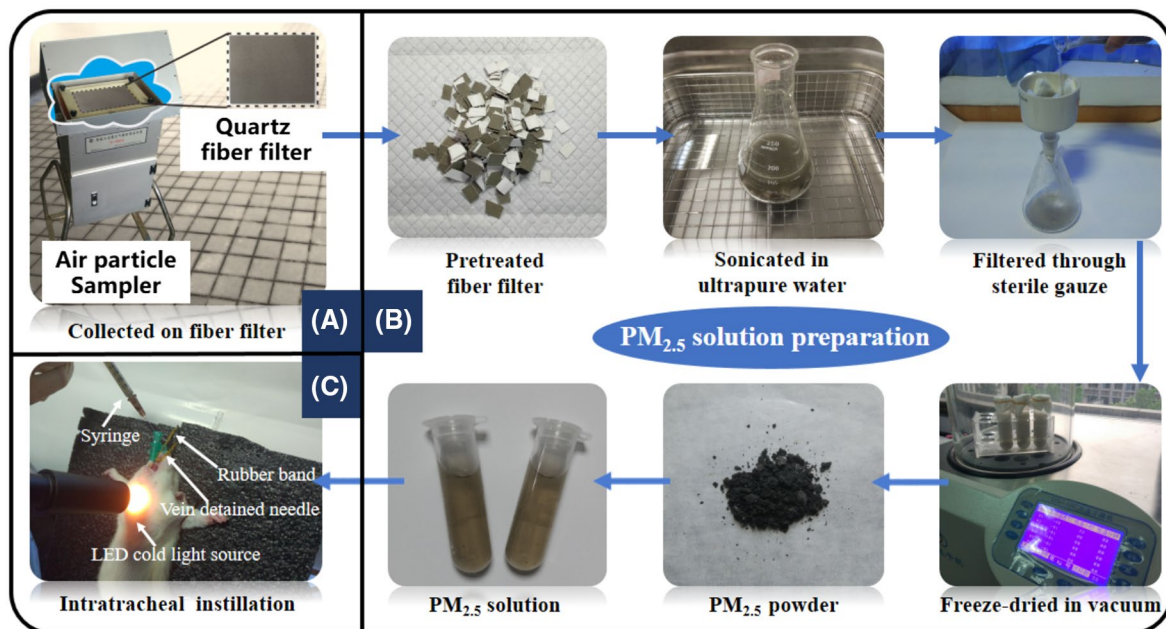

FIGURE 1   Schematic of PM$_{2.5}$ solution and animal model preparation. PM$_{2.5}$ was collected using a large-volume air particle sampler in Wuhan, China, as shown in (A). After collection, the PM$_{2.5}$ sample was purified and suspended in NS to obtain the PM$_{2.5}$ solution; the details are shown in (B). Next, the PM$_{2.5}$ solution was intratracheally instilled into the rat lung to build an animal model, as shown in (C). LED = light-emitting diode

2.5 | MR experiments

All the MR experiments were performed on a 7.0T animal MRI scanner (Bruker BioSpec 70/20 USR; Bruker, Ettlingen, Germany) using home-built double-tuned (^{1}H/^{129}Xe) birdcage coils with an inner diameter of 55 mm.

Both the CSSR and DWI sequences were used to acquire the pulmonary structure and functional data. For the CSSR experiments, two Gaussian pulses with durations of 0.5 and 0.2 ms were used to saturate and excite the dissolved ^{129}Xe signal, respectively.[39] The off-resonance effect of saturation and excitation pulses on the gas phase signal was approximately $0.1°$ and $0.9°$, respectively. Twenty-four exchange time points varying from 2 to 400 ms were used to acquire the dynamic spectra of the lung[39] in single breath-hold with a duration of 4 seconds. ^{129}Xe spectra were acquired using a bandwidth of 25 kHz with 1024 sampling points. Lungs were flushed with hyperpolarized xenon gas twice to remove the residual paramagnetic oxygen[39] for improving the signal-to-noise ratios (SNRs) of dissolved xenon signals, and the MR data were collected when rats inhaled xenon for the third time. Five sets of CSSR data were collected for each rat.

For DWI experiments, 2D diffusion-weight gradient echo imaging was used with the following parameters: ramp up/down time, 0.123 ms; constant time, 0.7 ms; diffusion time, 1.3 ms; matrix size, 64×64; field of view, 6×6 cm; flip angle, $10°$; bandwidth, 50 kHz; TE, 3.52 ms. Eight b values (4, 8, 12, 16, 20, 24, 28, and 32 s/cm^2) were used to fit the nonmonoexponential signal decay. In order to correct the influence of decreased xenon signal caused by radiofrequency excitation and T_1 relaxation on the diffusion-weighted images, interleaved sampling strategy was used,[28,43] and the images were acquired for a given line of k-space in the order of $b = 0$, x, 0 s/cm^2. Accordingly, for each b value, 3 images were collected in a single breath-hold with a duration of 4 seconds after lungs were flushed once using hyperpolarized xenon gas.

2.6 | Data processing

All the MR data were processed using MATLAB software (The MathWorks, Inc., Natick, MA). Amplitudes of the dissolved and gaseous xenon signal were extracted by fitting the CSSR data to the Lorentzian shape function.[44] Ratios of the xenon signal in RBCs or TP to the xenon signal in the alveoli were calculated using the extracted signal amplitudes. Next, amplitudes of the RBC and TP signals were normalized by the actual xenon gas signal in the alveoli[38,39,45,46] and were fitted to the gas exchange model of xenon exchange (MOXE).[47] The physiological parameters, including scaling factor (b), barrier-to-septum ratio (δ/d), exchange time constant (T), fraction of RBC xenon in blood (η), and pulmonary capillary transit time (t$_x$), were extracted from the fitting directly. Then, septal wall thickness (d), surface area to volume ratio (SVR), blood hematocrit (Hct), and thickness of air–blood barrier (δ) were obtained by the following equations: $d = \sqrt{\pi^2 DT}$, SVR $= 2b/(\lambda d)$, and Hct $= (\eta/\lambda_{RBC})/(\eta/\lambda_{RBC} + (1 - \eta)/\lambda_P)$, respectively, where D is the diffusion coefficient for xenon in lung tissue; λ, λ_{RBC}, and λ_P are the Ostwald solubilities of xenon in lung parenchyma, RBC, and plasma, respectively. For the DWI images, raw k-space data were directly reconstructed into images by performing an inverse Fourier transform. Before further processing, to obtain the whole ventilation map of the lung for DWI data fitting, two images without the diffusion gradient (i.e., $b = 0$) were averaged to generate a binary mask to segment the images. Then, SNRs of the segmented images were calculated by dividing the intensity of the pixels to the standard deviation (SD) of the noises in the image background, and only pixels with an SNR > 3 were used.[45] Next, to remove the main tracheal from the microstructure map and obtain the morphometric parameters of lung parenchyma, a seed-growing algorithm was used to segment the apparent diffusion coefficient (ADC) map of $b = 4$ s/cm^2, because the ADC values are larger in the main tracheal than that in the parenchyma.[43] The obtained mask was used to segment all 8 b-value images. After segmentation, morphometric parameter maps were generated by fitting the DWI data to the anisotropic diffusion model[48] of ^{129}Xe diffusion pixel by pixel using a nonlinear least-squares algorithm (Equation 14 in reference Sukstanskii and Yablonskiy[48]).

2.7 | Quantitative histology

Rats were sacrificed, and lungs were extracted immediately after MR experiments. Each extracted lung was preserved in 4% paraformaldehyde solution for more than 48 hours after it was filled to an airway pressure of 25 cm of H_2O with 4% paraformaldehyde solution for 2 hours. Thereafter, each lung was embedded in paraffin and cut into six 5-μm-thick tissue sections from a cross-section, which were stained with H&E to assess histological changes. For each section, 3 images that did not contain a large airway were acquired with a microscope (Nikon Eclipse Ts 100; Nikon Corporation, Tokyo, Japan). A standard test grid was overlaid on the image; septal thickness was determined as the average of the total truncated length.[49,50] For each rat, 18 images were used to automatically calculate alveolar septal thickness by Image-Pro Plus software (Media Cybernetics, Buckinghamshire, UK).[28,39,51]

2.8 | Statistical analysis

Statistical analysis was performed on all the data to evaluate the statistical significance between the control and PM$_{2.5}$

cohorts using an unpaired 2-tailed t test and SPSS software (IBM Corp., Armonk, NY) and PASW Statistics 18 (SPSS, Inc., Chicago, IL). P values < .05 determined significance.

3 | RESULTS

3.1 | Pulmonary function tests

Statistical analyses of the body-weight and pulmonary function parameters are summarized in Table 1. No significant difference was found in PFTs and body weight between the cohorts. However, in the PM$_{2.5}$ group, the FEV in 100 ms (FEV$_{100}$) decreased from 3.67 ± 0.52 to 3.51 ± 0.33 mL, and the FRC increased from 3.38 ± 1.46 to 3.74 ± 0.45 mL compared with that in the NS group.

3.2 | Hyperpolarized ^{129}Xe DWI

Figure 2 shows the representative morphological maps from the NS and PM$_{2.5}$ cohorts. Distributions of external radius (R), internal radius (r), alveolar sleeves of depth (h), mean

airspace chord length (Lm), and SVR derived from the cylindrical model[48] were homogeneous in the corresponding map. Statistics of the measured morphometric parameters and corresponding SDs for all rats are summarized in Table 2. No significant differences were found in these parameters between the NS and PM$_{2.5}$ groups.

3.3 | Hyperpolarized Xe CSSR

Mean ratios of RBC/GAS, TP/GAS, and RBC/TP in each group are shown in Figure 3, and peak amplitudes from the CSSR spectra at an exchange time of 100 ms were used to determine ratios.[39] TP/GAS ratio increased from 0.828 ± 0.115 to 1.019 ± 0.140 in the PM$_{2.5}$ cohort ($P = .021$). No significant difference was found in both the RBC/GAS (0.427 ± 0.064 for NS rats and 0.458 ± 0.141 for PM$_{2.5}$ rats) and RBC/TP ratios (0.492 ± 0.083 for NS rats and 0.443 ± 0.122 for PM$_{2.5}$ rats, showing a decreasing trend) between the groups.

Figure 4 shows the typical dissolved xenon signal recovery curves from the NS and PM$_{2.5}$ groups, respectively. In PM$_{2.5}$ rats, the normalized TP xenon signal increased clearly,

TABLE 1 Summary of the body-weight (BW) and pulmonary function tests in NS and PM$_{2.5}$ rats

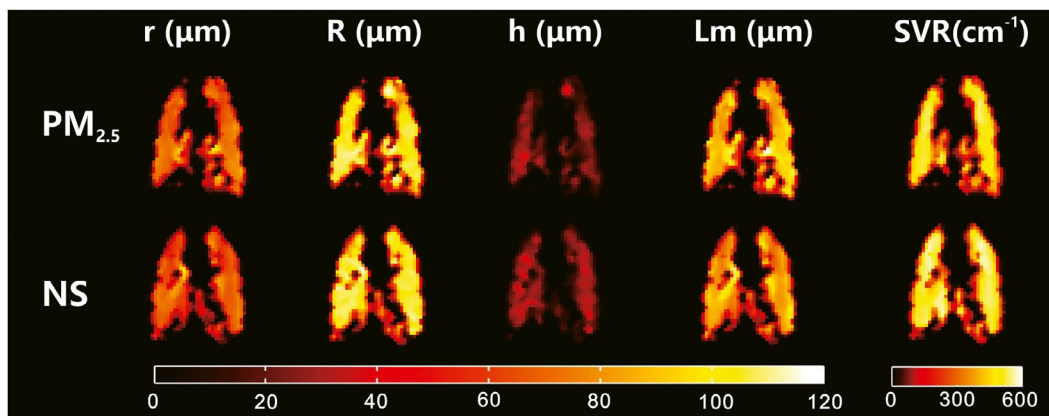| Parameters	Symbol	NS rats	PM$_{2.5}$ rats	P value
Body weight	BW (g)	283 ± 26	291 ± 21	.587
Forced vital capacity	FVC (mL)	9.80 ± 1.63	10.16 ± 1.20	.677
Functional residual capacity	FRC (mL)	3.38 ± 1.46	3.74 ± 0.45	.580
Total lung capacity	TLC (mL)	11.48 ± 1.86	11.76 ± 0.57	.733
Forced expiratory volume in 100 ms	FEV$_{100}$ (mL)	3.67 ± 0.52	3.51 ± 0.33	.540
Chord compliance (0~10 cm of H$_2$O)	Cchord (mL/cm H$_2$O)	0.72 ± 0.13	0.69 ± 0.09	.625

FIGURE 2 Representative maps of the microstructure from the NS (top row) and PM$_{2.5}$ rat groups (bottom row). All the maps of microstructural parameters are similar and homogeneous throughout the lung in both the NS and PM$_{2.5}$ groups; no significant differences were observed. All the microstructural parameters were derived from a hyperpolarized ^{129}Xe diffusion-weighted MRI model

TABLE 2 Morphometric parameters for each rat from the NS and PM$_{2.5}$ groups

Subject	R (µm)	r (µm)	h (µm)	Lm (µm)	SVR (cm^{-1})
NS rats					
1	104 ± 19	71 ± 12	33 ± 16	87 ± 18	475 ± 88
2	96 ± 18	62 ± 14	33 ± 15	77 ± 21	551 ± 120
3	102 ± 17	68 ± 11	34 ± 16	84 ± 17	495 ± 86
4	97 ± 18	57 ± 12	40 ± 17	71 ± 18	590 ± 106
5	99 ± 21	64 ± 15	35 ± 17	79 ± 21	533 ± 113
6	94 ± 17	60 ± 14	34 ± 14	74 ± 21	572 ± 119
Mean ± SD[a]	99 ± 4	64 ± 5	35 ± 3	79 ± 6	536 ± 44
PM$_{2.5}$ rats					
1	103 ± 20	75 ± 13	28 ± 15	94 ± 19	441 ± 87
2	97 ± 19	66 ± 13	32 ± 15	81 ± 20	517 ± 103
3	98 ± 19	59 ± 13	38 ± 17	73 ± 19	573 ± 110
4	100 ± 18	65 ± 14	35 ± 15	79 ± 20	530 ± 109
5	105 ± 18	68 ± 13	36 ± 16	84 ± 19	497 ± 95
6	96 ± 18	56 ± 14	40 ± 16	69 ± 19	609 ± 116
Mean ± SD[a]	100 ± 4	65 ± 7	35 ± 4	80 ± 9	528 ± 59
P value	0.770	0.571	0.923	0.734	0.785

[a]Morphometric parameter values were presented as the means ± SD of the whole lung for each rat.
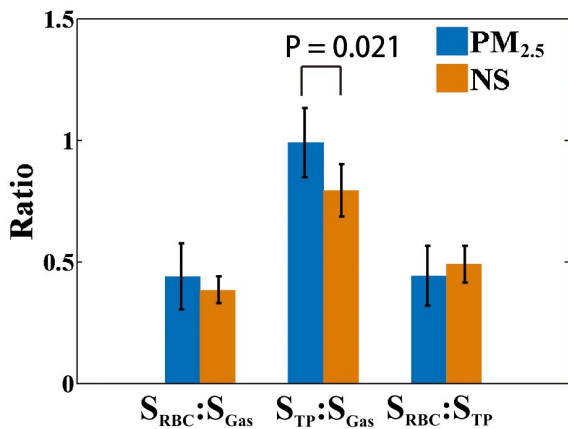

FIGURE 3 Comparison of RBC/GAS, TP/GAS, and RBC/TP (the signal ratios of RBC/GAS and TP/GAS in this figure are not normalized by the actual xenon gas signal) between the PM$_{2.5}$ and NS cohorts. A significantly higher TP/GAS ratio was found in the PM$_{2.5}$ group (*P* = .021)

whereas the normalized RBC xenon signal showed almost no difference. The extracted physiological parameters using MOXE are summarized in Table 3. The mean scaling factor increased significantly (*P* < .05), from 0.0175 ± 0.0006 in the NS group to 0.0214 ± 0.0011 in the PM$_{2.5}$ group. The measured mean SVR showed an increasing trend in PM$_{2.5}$ rats (318.10 ± 11.54 cm^{-1}) than NS rats (284.54 ± 9.16 cm^{-1}), but not significant. The exchange time constant (T) and septal wall thickness (d) of PM$_{2.5}$ rats increased significantly from 11.74 ± 2.39 to 14.00 ± 2.84 ms and from 6.17 ± 0.48 to 6.74 ± 0.52 µm.

3.4 | Histopathological observations in H&E-stained lung tissue

Figure 5 shows the H&E-stained lung physiological sections from typical NS and PM$_{2.5}$ rats, respectively. Neutrophil infiltration and thickening of alveolar walls could be observed in PM$_{2.5}$ rats, and septal thickness increased from 5.52 ± 0.32 to 6.20 ± 0.36 µm (*P* < .05).

4 | DISCUSSION

The influence of PM$_{2.5}$ on pulmonary microstructure and function was quantitatively and comprehensively evaluated using PFTs, quantitative histology, and hyperpolarized ^{129}Xe MR in this study. Significance differences were observed between the control and model groups treated by PM$_{2.5}$ in the pulmonary physiological function by hyperpolarized ^{129}Xe MRS. To our knowledge, this study was the first to demonstrate the feasibility and potential of hyperpolarized ^{129}Xe MR in evaluating pulmonary physiological changes caused by PM$_{2.5}$. Moreover, the potential of hyperpolarized ^{129}Xe CSSR in detecting early-stage lung disease related to PM$_{2.5}$ exposure was demonstrated. These findings may provide some useful suggestions to formulate environment protection strategies for countries such as China, wherein exposure to these kinds of air pollutants is a major health burden.

The mean exchange time constant (T) and septal thickness (d) showed a significant difference between PM$_{2.5}$ and
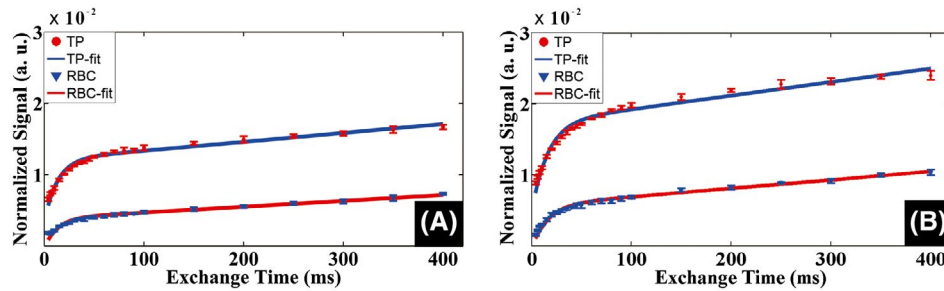
FIGURE 4 Dissolved xenon recovery curves of the representative NS rat (A) and PM$_{2.5}$ rat (B). Each point on the curve is averaged by 5 separate experiments. The dissolved xenon signals in PM$_{2.5}$ rat recovered slower and the TP signal increased significantly compared with that in the NS rat. a.u. = arbitrary units
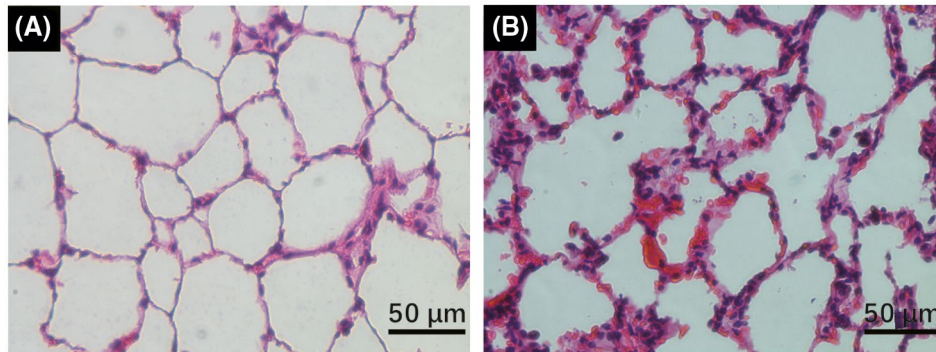

FIGURE 5 H&E-stained lung tissue from representative NS (A) and PM$_{2.5}$ rats (B). RBC exudation, neutrophil infiltration, and thickening of the alveolar wall were clearly observed in lungs of rats from the PM$_{2.5}$ group

TABLE 3 Physiological parameters of the lung obtained from the CSSR using MOXE

Parameter	Symbol	NS rats	PM$_{2.5}$ rats	*P* value
Scaling factor	b	0.0175 ± 0.0006	0.0214 ± 0.0011	.043[a]
Barrier-to-septum ratio	δ/d	0.14 ± 0.02	0.16 ± 0.05	.572
Exchange time constant	T (ms)	11.74 ± 2.39	14.00 ± 2.84	.045[a]
Fraction RBC xenon in blood	η	0.46 ± 0.04	0.44 ± 0.07	.657
Pulmonary capillary transit time	t_x (s)	0.55 ± 0.08	0.55 ± 0.10	.873
Septal wall thickness	d (μm)	6.17 ± 0.48	6.74 ± 0.52	.043[a]
Thickness of air–blood barrier	δ (μm)	0.86 ± 0.19	1.10 ± 0.46	.217
Surface area to volume ratio	SVR (cm^{-1})	284.54 ± 9.16	318.10 ± 11.54	.189
Blood hematocrit	Hct	0.29 ± 0.04	0.28 ± 0.06	.749

[a]At the 0.05 level, the differences in the population means were significantly different.

NS rats ($P < .05$), respectively, compared with those of NS rats. The parameters d and T showed a similar change trend because the value of d was derived from T by the equation $d = \sqrt{\pi^2 DT}$.[47] After treatment with PM$_{2.5}$, total septal thickness was approximately 1.1-fold larger than that in NS rats. The increase in the pulmonary septum and exchange time constant in PM$_{2.5}$ rats was most possibly caused by the exudation and infiltration of polymorphonuclear neutrophils, as reported in previous studies.[10,11,52] Thickening of the septal wall in PM$_{2.5}$ rats could also be observed in histology, as shown in Figure 5. Moreover, the measured septal thickness using hyperpolarized ^{129}Xe MR correlated well ($R^2 = 0.8$) with that using quantitative histology (shown in Figure 6).

TP/GAS ratio increased significantly ($P = .021$) in PM$_{2.5}$ rats, which is approximately 25% higher than that in
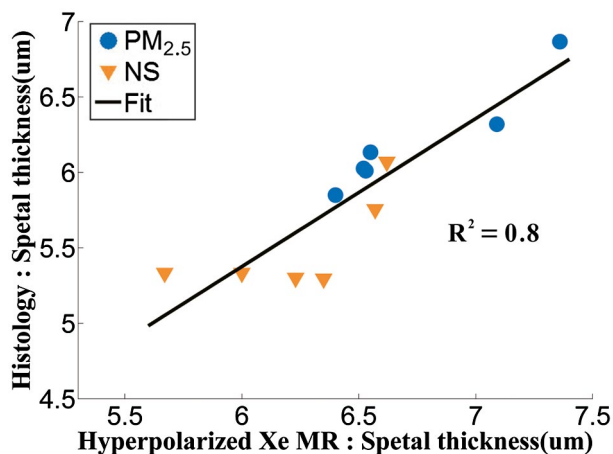
FIGURE 6 Correlation of septal thickness derived by hyperpolarized [129]Xe MR and histology. The solid line is the linear fit of the two methods, indicating that the septal thickness measured by the two methods had a good correlation ($R^2 = 0.8$)

NS rats. This is because the thickness of the septal wall was increased in $PM_{2.5}$ rats according to the histological results, and more xenon was dissolved in pulmonary tissue. The increased TP/GAS ratio is similar to that in previous studies, in which the increased TP/GAS ratio was caused by a thickened septal wall.[37-39,53,54] Meanwhile, no significant difference (<10%) was found in the RBC/GAS ratio between the $PM_{2.5}$ and NS rats. Aaron et al used CT to detect the increased volume of peripheral, smaller blood vessels in the lungs induced by $PM_{2.5}$,[14] but these blood vessels are not the main components of the pulmonary vasculature. Therefore, the small difference in RBC/GAS ratio between the $PM_{2.5}$ and NS cohorts may be attributed to biological variability and the stage of the $PM_{2.5}$ animal model in our study being relatively early. The small changes of blood vessels in rat lungs would be averaged in the whole-lung measurement of RBC/GAS ratio. This change may be exceeded by the individual differences between rats.

No significant difference was found in the measured morphological and PFT parameters between the cohorts. The most probable reason is that the stage of the $PM_{2.5}$ model was too early for PFTs and xenon gas DWI to be detectable. In a previous study,[11] lung compliance of $PM_{2.5}$ rats decreased significantly compared with that in control rats, and lung compliance also showed a similar trend in our study, but the difference was not significant between groups. A possible reason is that $PM_{2.5}$ model rats in the previous study showed more serious pulmonary injury when the concentration of $PM_{2.5}$ solution was 45 mg/kg, nearly 3 times higher than that in our study, and the larger dose of $PM_{2.5}$ would increase pulmonary inflammation and septum thickening.[10]

Our results indicate that the technique of hyperpolarized [129]Xe CSSR was more sensitive to the pulmonary physiological changes caused by $PM_{2.5}$. CSSR is a method to detect gas exchange function whereas PFTs and DWI can detect pulmonary structure changes. The $PM_{2.5}$ model is mild in our study, and PFTs or DWI could not distinguish changes in the pulmonary microstructure at such an early stage. However, pulmonary gas exchange could be detected between the groups by CSSR, indicating that the detectable physiological changes caused by $PM_{2.5}$ at the early stage are the parameters related to gas exchange.

The goal of this proof-of-concept study was intended to investigate the feasibility and potential of hyperpolarized [129]Xe MR in evaluating the impact of $PM_{2.5}$ on pulmonary microstructure and gas exchange function. Several limitations exist in this study. First, the animal models used in this study were induced by instilling $PM_{2.5}$ solution into rat lung to simulate long-term exposure to air pollution with $PM_{2.5}$ as reported in previous studies.[10-12,40,42,52] However, more studies involving variations to the particulate dose, dose administration timing, and incubation period are needed to fully understand the effects on the pulmonary system at large. In addition, it would be beneficial to investigate the effect on pulmonary function from chronic airborne exposure to pollutants using xenon MRI in the future, and the comparison of the methods for animal modeling should also be included in further studies. Second, pulmonary physiological status was evaluated on the seventh day after the instillation; more time points should be added to investigate the evolution of injury caused by $PM_{2.5}$. Third, as a concept-of-proof study, only whole-lung gas exchange was measured using CSSR; however, dissolved xenon imaging techniques should also be added for visualizing the heterogeneity of gas exchange caused by $PM_{2.5}$-related diseases in future studies.[21,55,56] Also, the diffusing capacity of the lungs for carbon monoxide should be added in future studies to comprehensively evaluate changes in gas exchange function caused by $PM_{2.5}$. Additionally, the specific components of $PM_{2.5}$ are unclear, and all $PM_{2.5}$ samples were collected in the same city. In future studies, $PM_{2.5}$ samples should be collected from different cities, and the specific components of $PM_{2.5}$ should be analyzed to help fully understand the influence of toxic fine particles on the pulmonary microstructure and gas exchange functions.

5 | CONCLUSION

In this proof-of-concept study, we demonstrated the feasibility of hyperpolarized [129]Xe MR in evaluating $PM_{2.5}$-induced pulmonary physiological changes for the first time. It was found that the technique of hyperpolarized [129]Xe CSSR is more sensitive to the functional changes caused by toxic fine particles in air than PFTs and xenon DWI, and the significant increase in the mean exchange time constant and thickness of the septal wall were found in $PM_{2.5}$ models. Additionally, the TP/GAS ratio in $PM_{2.5}$

rats also showed a significant difference compared with that in NS rats. These results indicated that hyperpolarized ^{129}Xe MR is a promising method in quantifying lung injury caused by PM$_{2.5}$ at the early stage, which would benefit the diagnosis and evaluation of clinical pulmonary diseases in the future.

ORCID

Xin Zhou 🆔 https://orcid.org/0000-0002-5580-7907

REFERENCES

1. Lim SS, Vos T, Flaxman AD, et al. A comparative risk assessment of burden of disease and injury attributable to 67 risk factors and risk factor clusters in 21 regions, 1990–2010: a systematic analysis for the Global Burden of Disease Study 2010. *Lancet*. 2012;380:2224–2260.
2. Chen Z, Wang JN, Ma GX, Zhang YS. China tackles the health effects of air pollution. *Lancet*. 2013;382:1959–1960.
3. Guan WJ, Zheng XY, Chung KF, Zhong NS. Impact of air pollution on the burden of chronic respiratory diseases in China: time for urgent action. *Lancet*. 2016;388:1939–1951.
4. Xing YF, Xu YH, Shi MH, Lian YX. The impact of PM (2.5) on the human respiratory system. *J Thorac Dis*. 2016;8:E69–E74.
5. Guo Y, Zeng H, Zheng R, et al. The association between lung cancer incidence and ambient air pollution in China: a spatiotemporal analysis. *Environ Res*. 2016;144:60–65.
6. Lin HH, Murray M, Cohen T, Colijn C, Ezzati M. Effects of smoking and solid-fuel use on COPD, lung cancer, and tuberculosis in China: a time-based, multiple risk factor, modelling study. *Lancet*. 2008;372:1473–1483.
7. Dominici F, Peng RD, Bell ML, et al. Fine particulate air pollution and hospital admission for cardiovascular and respiratory diseases. *JAMA*. 2006;295:1127–1134.
8. Pope CA, Burnett RT, Thun MJ, et al. Lung cancer, cardiopulmonary mortality, and long-term exposure to fine particulate air pollution. *JAMA*. 2002;287:1132–1141.
9. Xu Z, Li Z, Liao Z, et al. PM (2.5) induced pulmonary fibrosis in vivo and in vitro. *Ecotox Environ Safe*. 2019;171:112–121.
10. Wang G, Zhao J, Jiang R, Song W. Rat lung response to ozone and fine particulate matter (PM (2.5)) exposures. *Environ Toxicol*. 2015;30:343–356.
11. Zhang S-Y, Shao D, Liu H, et al. Metabolomics analysis reveals that benzo[a]pyrene, a component of PM (2.5), promotes pulmonary injury by modifying lipid metabolism in a phospholipase A2-dependent manner in vivo and in vitro. *Redox Biol*. 2017;13:459–469.
12. Cao Q, Zhang S, Dong C, Song W. Pulmonary responses to fine particles: differences between the spontaneously hypertensive rats and wistar kyoto rats. *Toxicol Lett*. 2007;171:126–137.
13. Kong H, Xia K, Pan L, et al. Autophagy and lysosomal dysfunction: a new insight into mechanism of synergistic pulmonary toxicity of carbon black-metal ions co-exposure. *Carbon*. 2017;111:322–333.
14. Aaron CP, Hoffman EA, Kawut SM, et al. Ambient air pollution and pulmonary vascular volume on computed tomography: the MESA Air Pollution and Lung cohort studies. *Eur Respir J*. 2019;53:1802116.

15. Marshall J. PM 2.5. *Proc Natl Acad Sci USA*. 2013;110:8756–8756.
16. Albert MS, Cates GD, Driehuys B, et al. Biological magnetic-resonance-imaging using laser polarized Xe-129. *Nature*. 1994; 370:199–201.
17. Ruppert K, Hamedani H, Amzajerdian F, et al. Assessment of pulmonary gas transport in rabbits using hyperpolarized xenon-129 magnetic resonance imaging. *Sci Rep*. 2018;8:7310.
18. Thomen RP, Quirk JD, Roach D, et al. Direct comparison of Xe-129 diffusion measurements with quantitative histology in human lungs. *Magn Reson Med*. 2017;77:265–272.
19. Thomen RP, Walkup LL, Roach DJ, et al. Hyperpolarized Xe-129 for investigation of mild cystic fibrosis lung disease in pediatric patients. *J Cyst Fibros*. 2017;16:275–282.
20. Matin TN, Rahman N, Nickol AH, et al. Chronic obstructive pulmonary disease: lobar analysis with hyperpolarized Xe-129 MR imaging. *Radiology*. 2017;282:857–868.
21. Ruppert K, Amzajerdian F, Hamedani H, et al. Rapid assessment of pulmonary gas transport with hyperpolarized Xe-129 MRI using a 3D radial double golden-means acquisition with variable flip angles. *Magn Reson Med*. 2018;80:2439–2448.
22. Gimi B, Molthen RC, Guo F, et al. Automated pulmonary lobar ventilation measurements using volume-matched thoracic CT and MRI. *Proc SPIE Int Soc Opt Eng*. 2015;9417:941717.
23. He M, Driehuys B, Que LG, Huang YT. Using hyperpolarized Xe-129 MRI to quantify the pulmonary ventilation distribution. *Acad Radiol*. 2016;23:1521–1531.
24. Chan HF, Stewart NJ, Parra-Robles J, Collier GJ, Wild JM. Whole lung morphometry with 3D multiple b-value hyperpolarized gas MRI and compressed sensing. *Magn Reson Med*. 2017; 77:1916–1925.
25. Ouriadov A, Lessard E, Sheikh K, Parraga G. Canadian Respiratory Research N. Pulmonary MRI morphometry modeling of airspace enlargement in chronic obstructive pulmonary disease and alpha-1 antitrypsin deficiency. *Magn Reson Med*. 2018;79: 439–448.
26. Wang W, Nguyen NM, Yablonskiy DA, et al. Imaging lung microstructure in mice with hyperpolarized He-3 diffusion MRI. *Magn Reson Med*. 2011;65:620–626.
27. Zhang H, Xie J, Xiao S, et al. Lung morphometry using hyperpolarized Xe-129 multi-b diffusion MRI with compressed sensing in healthy subjects and patients with COPD. *Med Phys*. 2018;45:3097–3108.
28. Ruan W, Zhong J, Guan Y, et al. Detection of smoke-induced pulmonary lesions by hyperpolarized Xe-129 diffusion kurtosis imaging in rat models. *Magn Reson Med*. 2017;78:1891–1899.
29. Sakai K, Bilek AM, Oteiza E, et al. Temporal dynamics of hyperpolarized Xe-129 resonances in living rats. *J Magn Reson Series B*. 1996;111:300–304.
30. Stewart NJ, Horn FC, Norquay G, et al. Reproducibility of quantitative indices of lung function and microstructure from Xe-129 chemical shift saturation recovery (CSSR) MR spectroscopy. *Magn Reson Med*. 2017;77:2107–2113.
31. Ruppert K, Brookeman JR, Hagspiel KD, Driehuys B, Mugler JP. NMR of hyperpolarized Xe-129 in the canine chest: spectral dynamics during a breath-hold. *NMR Biomed*. 2000;13: 220–228.
32. Ruppert K, Brookeman JR, Hagspiel KD, Mugler JP. Probing lung physiology with xenon polarization transfer contrast (XTC). *Magn Reson Med*. 2000;44:349–357.

33. Driehuys B, Cofer GP, Pollaro J, et al. Imaging alveolar-capillary gas transfer using hyperpolarized Xe-129 MRI. *Proc Natl Acad Sci USA*. 2006;103:18278–18283.

34. Mugler JP, Altes TA, Ruset IC, et al. Simultaneous magnetic resonance imaging of ventilation distribution and gas uptake in the human lung using hyperpolarized xenon-129. *Proc Natl Acad Sci USA*. 2010;107:21707–21712.

35. Fox MS, Ouriadov A, Thind K, et al. Detection of radiation induced lung injury in rats using dynamic hyperpolarized Xe-129 magnetic resonance spectroscopy. *Med Phys*. 2014;41:072302.

36. Imai H, Kimura A, Iguchi S, et al. Noninvasive detection of pulmonary tissue destruction in a mouse model of emphysema using hyperpolarized Xe-129 MRS under spontaneous respiration. *Magn Reson Med*. 2010;64:929–938.

37. Qing K, Mugler JP III, Altes TA, et al. Assessment of lung function in asthma and COPD using hyperpolarized Xe-129 chemical shift saturation recovery spectroscopy and dissolved-phase MRI. *NMR Biomed*. 2014;27:1490–1501.

38. Stewart NJ, Leung G, Norquay G, et al. Experimental validation of the hyperpolarized Xe-129 chemical shift saturation recovery technique in healthy volunteers and subjects with interstitial lung disease. *Magn Reson Med*. 2015;74:196–207.

39. Li H, Zhang Z, Zhao X, et al. Quantitative evaluation of radiation-induced lung injury with hyperpolarized xenon magnetic resonance. *Magn Reson Med*. 2016;76:408–416.

40. Wang G, Jiang R, Zhao Z, Song W. Effects of ozone and fine particulate matter (PM (2.5)) on rat system inflammation and cardiac function. *Toxicol Lett*. 2013;217:23–33.

41. Wang H, Song L, Ju W, et al. The acute airway inflammation induced by PM2.5 exposure and the treatment of essential oils in Balb/c mice. *Sci Rep*. 2017;7:44256.

42. Zhang Y, Hu H, Shi Y, et al. H-1 NMR-based metabolomics study on repeat dose toxicity of fine particulate matter in rats after intratracheal instillation. *Sci Total Environ*. 2017;589:212–221.

43. Ruan W, Zhong J, Wang KE, et al. Detection of the mild emphysema by quantification of lung respiratory airways with hyperpolarized xenon diffusion MRI. *J Magn Reson Imaging*. 2017;45:879–888.

44. Chang YV, Quirk JD, Ruset IC, et al. Quantification of human lung structure and physiology using hyperpolarized Xe-129. *Magn Reson Med*. 2014;71:339–344.

45. Zhong J, Zhang H, Ruan W, et al. Simultaneous assessment of both lung morphometry and gas exchange function within a single breath-hold by hyperpolarized Xe-129 MRI. *NMR Biomed*. 2017;30:e3730.

46. Zhong J, Ruan W, Han Y, et al. Fast determination of flip angle and T1 in hyperpolarized gas MRI during a single breath-hold. *Sci Rep*. 2016;6:25854.

47. Chang YV. MOXE: a model of gas exchange for hyperpolarized Xe-129 magnetic resonance of the lung. *Magn Reson Med*. 2013;69:884–890.

48. Sukstanskii AL, Yablonskiy DA. Lung morphometry with hyperpolarized Xe-129: theoretical background. *Magn Reson Med*. 2012;67:856–866.

49. Pua ZJ, Stonestreet BS, Cullen A, et al. Histochemical analyses of altered fetal lung development following single vs multiple courses of antenatal steroids. *J Histochem Cytochem*. 2005;53:1469–1479.

50. Woods JC, Choong CK, Yablonskiy DA, et al. Hyperpolarized 3He diffusion MRI and histology in pulmonary emphysema. *Magn Reson Med*. 2006;56:1293–1300.

51. He M, Cheng NI, Gao W-W, et al. Characterization of Quin-C1 for its anti-inflammatory property in a mouse model of bleomycin-induced lung injury. *Acta Pharmacol Sin*. 2011;32:601–610.

52. Riva DR, Magalhães CB, Lopes AA, et al. Low dose of fine particulate matter (PM (2.5)) can induce acute oxidative stress, inflammation and pulmonary impairment in healthy mice. *Inhal Toxicol*. 2011;23:257–267.

53. Kaushik SS, Freeman MS, Yoon SW, et al. Measuring diffusion limitation with a perfusion-limited gas-hyperpolarized Xe-129 gas-transfer spectroscopy in patients with idiopathic pulmonary fibrosis. *J Appl Physiol*. 2014;117:577–585.

54. Wang JM, Robertson SH, Wang ZY, et al. Using hyperpolarized Xe-129 MRI to quantify regional gas transfer in idiopathic pulmonary fibrosis. *Thorax*. 2018;73:21–28.

55. Qing K, Ruppert K, Jiang Y, et al. Regional mapping of gas uptake by blood and tissue in the human lung using hyperpolarized xenon-129 MRI. *J Magn Reson Imaging*. 2014;39:346–359.

56. Zanette B, Santyr G. Accelerated interleaved spiral-IDEAL imaging of hyperpolarized (129) Xe for parametric gas exchange mapping in humans. *Magn Reson Med*. 2019;82:1113–1119.